Nanostructured Supported Palladium Catalysts – Non-oxidative Methane Coupling

Silvia F.Moya[1], Ruth L.Martins[1], Antje Ota[2], Edward L. Kunkes[2], Robert Schlögl[2], Malte Behrens[2], Martin Schmal[1]*

[1] Federal University of Rio de Janeiro, Programa de Engenharia Química / COPPE/NUCAT, Cidade Universitária - CP: 68502, Rio de Janeiro, RJ, 21941-972, Brasil,

[2] Fritz Haber Institute, Department of Inorganic Chemistry, Faradayweg 4-6, 14195 Berlin, Germany

*Corresponding author; schmal@peq.coppe.ufrj.br., Fax 55-21-2562-8360

1. Introduction

The non-oxidative conversion of methane in a two step reaction has been suggested as an alternative to the oxidative coupling of methane [1]. This reaction leads to coupling products and comprises the chemisorption of methane and the reaction of the carbon adspecies on a noble metal catalyst with hydrogen. The nature and reactivity of the adspecies formed after the methane chemisorption step are expected to be different dependent on the reaction conditions. Studies of methane chemisorption at moderate temperatures and the decomposition to carbon adspecies and H_2 at higher temperatures have been reported in the literature [1-7]. An important comparative study concerning methane activation was presented by Guczi and Borko [8] using the hydrogen-assisted one-step methane conversion over Pd-Co/SiO_2 and Pt-Co/NaY catalysts. We have reported the non-oxidative conversion of methane, through the isothermal two step reaction on Pt loaded catalysts [9]. The reaction was conducted in pulse and continuous modes. In a flow mode operation, methane chemisorption is followed by the evolution of H_2, plus $C_2^{=}$, C_2, $C_3^{=}$, and C_3, depending on the nature of the support. The hydrogenation of carbon residues produced mainly methane, but ethane and propane were also detected.

Ma et al [10] showed that the activation during chemisorption and hydrogenation depends on the dispersion of the catalytic metal. On Pt-PVP/Hβ the amount of methane homologation increased with smaller particles and that the distribution of C_2^+ to higher hydrocarbons decreased. Therefore, the influence of the morphology, crystalline, location of atoms on vertices and kinks may affect the activity and selectivity in this reaction.

Clusters, grains, lamellar structures or filaments with dimensions smaller than 10 nm can be considered as nanostructured materials. These systems present a high ratio of surface area and volume with singular properties. In catalysis they may change electronic structures at the surface which influences the reactivity differing completely from the conventional

systems, such as surface dynamics, sintering, reactivity and selectivity. Therefore, structure sensitive reactions are strongly influenced by particle sizes and, thus, on the method of preparation of the supported metal catalyst [11-14], for example, in the FT synthesis, using Fe/SiO_2. Nanoparticles of Pd supported on α-Al_2O_3 were synthesized by Okitsu [12] using as precursor $(PdCl_4)^{-2}$. The authors claim that the particles supported were first nucleated as reduced Pd species, followed by growth in the solution and finally anchoring on the support. Compared to the conventional impregnation method of preparation the activity for hydrogenation was 20 times better.

Miyazaki et al. (15) prepared Pt nanoparticles using colloids. This is a very interesting method of preparation, because it allows controlling variables to obtain small particles. These authors prepared the catalyst using as precursor K_2PtCl_4 reduced with H_2 and using three stabilizers. They obtained particles of the order or 6.9 to 14.6nm, using PVP (poly *N*-isopropylacrilamid), NIPA and SPA (sodium poly-acrylate), as stabilizers, respectively.

The main objective of this work is to study the influence of the preparation method of nanostructured supported palladium catalysts over α-Al_2O_3 in the non-oxidative methane coupling. Two catalysts were prepared by the sonochemistry and colloidal solution with polymeric stabilizers methodologies, comprehensively characterized and tested in the non-oxidative methane activation by chemisorption and hydrogenation in two sequential steps.

2. Experimental

Palladium supported catalysts were prepared by different methodologies on uncalcined α-Al_2O_3 support (Norton). Elemental analysis results in a silica content of 6 wt%. The first sample was prepared using the sonochemical method, as suggested by Okitsu et al., [16]. Thus, 1 % Pd/α-Al_2O_3 (named PdSON) sample was prepared starting with a solution of 6.2×10^{-2} mmol $PdCl_2$ (Aldrich), saturated with air in the Erlenmeyer and addition of 0.2 μL of isopropanol (C_3H_8O, Vetec). This solution was placed in the ultrasonic bath (Bransonic,

Ultrasonic Cleaner 452E at 50/60 Hz, 117 V, 1.0 A) and submitted to radiation for 30 minutes. The final material was filtered, washed with deionized water and dried in a muffle at 120^0C for 20 h. The sample was stored in a desiccator.

The second sample (1 % Pd/α-Al_2O_3) was prepared with a colloidal solution and reduced in solution in the presence of a stabilizer, using a polymeric ligand. First, a solution of 2 mmol.L^{-1} of H_2PdCl_4 was prepared and added to this solution 0.067 g of PVP and 0.5 mL of chloride acid with 21 mL deionized water. The mixture was washed with reflux under Ar atmosphere. Then, 14 ml of ethanol was added and refluxed for 3 h, cooled and stored in a mixture of water and ethanol. Nanoparticles were obtained over the support after evaporation of the solution in a rotavapor. The residual solvent was removed by drying in a muffle for 24 h (Pd-COL. The polymer was removed by calcination at 663 K after pretreatment with 5%O_2/He and 60 ml/min. (Table 1) and named PdCOL.

2.1 Characterizations:

Elemental chemical analysis on a X-ray fluorescence (XRF) Rigaku spectrometer, RIX 3100 apparatus. The specific surface area was determined by BET method, using N_2 adsorption at liquid nitrogen temperature, using a Micromeritics ASAP 2000 apparatus. Before analysis, the samples were degassed for 24 h at 473K in vacuum.

X-ray diffraction (XRD)

The crystalline phases were evaluated by in situ X-ray diffraction (XRD) using the powder method and Cu Kα radiation. The diffraction patterns were recorded on a Rigaku DMax 2200 diffractometer. The diffratograms were recorded in the range of $2º \leq 2\theta \leq 120º$ with 0.05º and speed of 0.15 ^{0}.min^{-1}.

Temperature-programmed Desorption (TPD)

Electronic microscopy – TEM and SEM

SEM images were recorded in a field emission scanning electron microscope (Jeol JSM) model 6460LV, working at 20 kV. The sample preparation consisted of dispersing the catalyst in powder form on a carbon film conductor. The images were obtained without the need to cover the sample with gold.

Transmission electron microscopy (TEM) was carried out in a JEM 3010 microscope, operating with acceleration voltage of 300 kV. The sample was suspended in isopropyl alcohol and dropped in a holey carbon coated copper grid before the TEM analysis.

Diffuse reflectance spectroscopy with infrared Fourier transform (DRIFTS) of CO adsorption.

The tests were performed on a Nicolet spectrometer, model Nexus 470 (resolution 4 cm^{-1} and MCT-A detector), equipped with an accessory for diffuse reflectance Spectra-Tech and windows of ZnSe. The samples, undiluted or packed were treated in situ. The reduction was performed with pure hydrogen at 30 ml/min and 5 K/min up to 773 K. Then, swept to He flow at 30 mL. min^{-1} and cooled to room temperature. After pre-treatment a mixture of 5% CO in He was introduced in the chamber at room temperature. Spectra were obtained after 1 and 15 min in flowing CO. Then, by closing the chamber a spectrum was obtained after 15 min and swept to He flow for 10 min to eliminate physisorbed CO. The spectra were obtained after desorption at different temperatures 323, 373, 423, 473 and 573 K.

2.2 Methane coupling reaction in two stages

Methane chemisorption and hydrogenation of carbon adspecies

Methane chemisorption and hydrogenation of carbon adspecies at the surface of the metal were conducted at atmospheric pressure in a Pyrex micro reactor fixed bed with a valve coupled to multi-loops equipped with 16 loops, as described in [17]. Aliquots of the effluent gases of the chemisorption and hydrogenation steps were stored in different loops to be further analyzed in the gas chromatograph coupled online to a Varian, model CP-3800 GC. It was equipped with CP Poraplot Q column, operating at isothermal condition in the first 15 min of analysis, then heated at 20 K/min up to 473 K and held at this temperature for 18 min under isobaric condition. He was used as carrier gas. The products were analyzed by flame ionization detector (FID).

Before carrying out the catalytic tests the catalysts were pre-treated with pure hydrogen at 60 mL/min and temperature rising at 5 K/min up to 773 K. He passed at this temperature to remove traces of H_2 at the metal surface. After cooling (in He flow) to the temperature of adsorption it was swept to pure methane at 300 ml/min for 1 min. At the end He passed at high flow rate for 5 min to clean the surface before the hydrogenation step. The hydrogenation was carried out isothermally during 1 min with pure H_2 flowing at 60 ml/min Then, it was heated up under reductive atmosphere until the temperature of reduction and kept for 20 minutes to remove all C species not hydrogenated in the isothermal step. Finally, it was cooled and repeated for the entire range of temperature.

The activity of the catalysts was evaluated in the temperature range 373 - 873 K. The mass was 300 mg catalyst.

Temperature Programmed Surface Hydrogenation (TPSH)

The TPSH analysis was done for quantifying the adsorbed methane. It was carried out in the equipment described elsewhere [17]. In short, it consists of a quartz tube, connected to a thermocouple for monitoring the temperature and a furnace controlled by a temperature

programmer. The effluent gases were analyzed by coupling the Balzers quadrupole mass spectrometer PRISMA and a computer for data acquisition. The experiment was based on the simulation of the adsorption step of methane carried out in the catalytic test; however, the hydrogenation proceeded varying the temperature from room up to an appropriate temperature that ensures that all adsorbed methane was hydrogenated.

The mass of the catalyst was also 300 mg. Firstly the catalyst was reduced at 773 K with pure hydrogen at 60 ml/min and at 5 K/min. Then, swept to He flow to remove H_2 traces on the metal surface and cooled under He flow to a fixed temperature for chemisorption of methane (553, 673 and 773 K). Once reached the correct temperature, methane was admitted at a flow rate of 300 ml/min over a period of one minute. At the end the reactor was sealed and cooled to room temperature over a period of 120 min to prevent aging of wastes formed at the surface at high temperatures. The excess of methane in the reactor was eliminated flowing pure He at 60 mL/min for 40 min before data acquisition. In the sequence, H_2 was admitted at 60 ml/min and the reactor heated at 20 K/min up to 773 K and held at this temperature for 20 min. The temperature rose up to 1073 K. This temperature was held until the signal measured by the mass spectrometer returned to the baseline. Ratios of e/m were monitored related to methane, ethane, ethylene, propane and propene, CO and CO_2 as described previously in [17].

3. Results and discussion

The experimentally determined Pd content was 0.8% (mass) and when compared to theoretical content (1%) and the conventional Pd impregnation method we noticed that there is only a minor loss of Pd during the preparation of nano sized Pd particles by the sonification method.

Figure 1 displays the diffractogram of the Pd-SON sample showing three phases relative to α-Al_2O_3, besides silicate and mullite ($Al_6Si_2O_{13}$). Silicon was expected and observed in the chemical analysis presenting 6% (mass) of SiO_2, which is normally present in the alumina. Crystalline silicates were not observed in the support material before sonication (red line in the inset of Fig. 1) suggesting that crystallization occurred as a result of the energy input during sonication. The diffraction peaks of Pd are very small, but clearly seen when expanded in a small range between 35^o and 48^o and compared to the Pd free support (Fig. 1 inset). The most intense (111) line of metallic Pd is observed at 2θ=40.07 °.

It is worth noting that after storage in air the metallic palladium formed during synthesis remains metallic and is not oxidized. The diffraction line is slightly shifted to lower values corresponding to an expansion of the lattice parameter. The bulk palladium should present an intense diffraction line at 40.36^0, but on this sample it was shifted to 40.07^0. The detail shows the diffraction line of the plane corresponding to Pd (200) phase. The mean crystallite size was calculated using Scherer equation and the (111) peak of Pd. The calculated value was 6.0 nm.

Figure 2 displays the diffraction patterns of the support (A) and the PdCOL catalyst before calcinations (B) and after calcination (C). It shows the diffraction pattern of well crystallized α-Al_2O_3. However, if we expand this diffractogram it is possible to verify the presence metallic palladium in the uncalcined and calcined sample , which appears at 39.7^0 in a broad line and at 46.1^0 (with an asymmetric line at 46.5^0) and can be attributed to the planes (111) and (200) of cubic structure. These lines are slightly shifted when compared to bulk palladium and indicate variation of the lattice parameters. The estimated mean size of the crystallites is 7.2 nm for the uncalcined sample and 9.2 nm for the calcined sample suggesting that sintering of the Pd nanoparticles upon thermal removal of the stabilizer ligands occurs only to a minor degree.

TEM results

The TEM analyses were obtained after preparation and reduction of the PdSON catalyst. Figure 3 shows the images after preparation and Figure 4 after the reduction. Figure 3 shows particles with uniform sizes and in detail (right) the image of particles of higher magnification which are of the order of 5 to 10 nm.

Figure 4 shows the images after reduction where the particle sizes are significantly smaller and homogeneously distributed over the support, probably due to the dispersion and migration of particles during the reduction process. Note that with higher magnification in Figure 4 (below) the particles contain clusters of Pd particles at the surface of the alumina support. Figure 5 shows the images of the calcined and reduced PdCOL sample. Figure 6A presents the histogram of Pd particles after reduction of the PdSON catalyst, indicating that 70% of these particles are of the order of 6-9 nm, which is in good agreement with particle sizes of 6 nm, obtained by XRD. Figure 6B shows the histogram of the PdCOL sample. The metallic particles are very small, some less than 10nm, however, the image of the calcined sample (A) shows distribution of particles in the range of 2 to 30 nm. There are very small particles at the surface of the order of 10 nm. Compared to the PdSON sample the distribution of particles sizes is less uniform.

The Pd colloidal sample presents a tendency of grouping particles on α-Al_2O_3, which is very common on samples with high metallic dispersion, since these materials in nanometric scale exhibit high surface energy and the aggregation decreases the total energy. The α-Al_2O_3 is non porous material with low surface area that favors the formation of particle islands, as shown in figure 5, before calcination.

Drifts of CO adsorption

These experiments were performed to confirm the presence of an exposed metallic surface of the particles. Figure 7A displays the CO adsorption on the PdCOL sample after calcination and reduction. It shows CO linearly adsorbed on metallic Pd^0 at 2077 cm^{-1} with an asymmetric contribution at 2048 cm^{-1}. The broad band between 2000 cm^{-1} and 1850 cm^{-1}, shows a band at 1923 cm^{-1}, with a shoulder at 1948 cm^{-1}. This band suggests CO bridged adsorption band on metallic Pd^0. After heating at 373 K these bands disappear (not shown). The linear band is assigned to weak CO adsorption at the surface [18].

The spectrum of the PdSON sample (Figure 7B) displays two bands at 2090 cm^{-1} and a broad band around at 1930 cm^{-1}. The first one is attributed to the linear CO adsorption on metallic Pd^0, while the second band to CO bridged adsorption on Pd metallic species [19, 20]. Heating up to 373 K the linear CO adsorption band disappears and the CO bridged band decreased sharply, disappearing after heating up to 423 K. It seems that the CO linear adsorption band is associated to the highly dispersed metallic Pd^0 over the support.

There are significant differences in the intensities but the predominant adsorption is the linear CO adsorption band, suggesting CO adsorption located on kinks and planes of low coordination with defects at the surface. However, the PdSON displayed preferential linear adsorption band, thus higher metallic dispersion compared to the PdCOL sample which displays a less intense linear CO adsorption and bridged adsorption on Pd metallic species , and therefore lower dispersion of the metallic phase.

These results agree with TEM observations on PdCOL and PdSON samples. The PdSON exhibited small clusters and mean sizes of 10 nm, but very small particles spread at the surface. The PdCOL evidenced particle sizes around 20 nm and surface density apparently lower than for PdSON.

TPD of CO

TPD was performed after adsorption of 5%CO/He flow (at 30mL/min) on reduced sample. The temperature raised under He flow from room temperature to 773 K. The TPD profiles are shown in figure 8A and 8B.

Figure 8A displays the desorption profiles of the PdSON sample, showing a CO desorption peak at 378 K with a shoulder at 441 K, associated with this peak release of CO_2 at 476 K. The CO_2 may be assigned to the disproportionation reaction and thus deposition of carbon at the surface [21, 22. 23].

$2CO \rightarrow CO_2 + C_S$

These results indicate metallic Pd at the surface, in accordance with DRIFTS results. Most of the CO is weakly bound and desorbs before undergoing the disproportionation reaction. However, with increasing temperature metallic sites are covered by carbon species.

Figure 8B displays the CO TPD profile of the PdCOL sample, exhibiting a broad line between 350 K and 680 K and simultaneously releasing of CO_2 and H_2 above 658 K. It also indicates the presence of metallic palladium at the surface for a large extension of temperature. The broad and undefined signals compared to PdSON may be due to the lower homogeneity of the metallic Pd phase in this sample. However, the larger formation of CO_2 can be explained by the desproportionation reaction and decomposition of carbonates formed during the CO adsorption on the support. CO desorption begins at higher temperature compared to Pd-SON and occurs simultaneously with CO_2 desorption. Thus, CO seems to be more strongly bound, which favors the desproportionation reaction at higher temperatures. The H_2 released at 658 K is probably associated to the shift reaction due to the presence of water on the support [24].

$CO + H_2O \rightarrow CO_2 + H_2$

Temperature programmed surface hydrogenation (TPSH)

The first step of the homologation reaction is the adsorption of methane, followed by the hydrogenation step. According to the literature [25] during the adsorption of methane there are different surface carbon adspecies, which can be hydrogenated. The C_α adspecies, which can be hydrogenated at temperatures below 423 K, are highly active and predominant. The C_β and C_γ phases may be hydrogenated at higher temperatures. However, the γ phase is in dynamic equilibrium with other phases and originates predominantly from aging of chemisorbed methane species at the surface, which can be quickly converted to C species. Most of the carbon deposits hang and may form such "bad carbon" that by completion of several cycles of chemisorption of CH_4 / hydrogenation leads to catalyst deactivation. There is a possibility of aging carbon residues, as reported in the literature [26]. The carbon residue C_α (carbidic) may be transformed in amorphous carbon C_β which in turn can be transformed in C_γ adspecies [25, 27]. These carbon adspecies at the surface are not easily reduced.

The results are presented in Figures 9 and 10 and show signal of CH_4 evolved during the TPSH experiment for both catalysts and for different adsorption temperatures, 573, 673 and 773 K. The PdSON sample displayed different maxima peaks, which are shifted to higher temperature with increasing adsorption temperature, as shown in Figure 9. The maximum temperatures were 506, 546 and 623 K, respectively. The results show that carbon residues over the surface of PdSON become less reactive to hydrogenation with increasing adsorption temperature. The effect of decreasing reactivity of surface carbon species as a function of temperature on adsorption was observed by Koerts et al. [25] involving metal catalysts of group VIII. The PdCOL sample exhibited a signal of CH_4 and different profiles with maxima at equal temperature 527 K for different adsorption temperatures, as shown in Figure 10, besides a band at higher temperature. It suggests the reaction of the same carbon adspecies,

which may be attributed to the amorphous carbon phase. In this case, the nature of C adspecies is less influenced by chemisorption temperature [25]. However, for the adsorption temperature at 673 K, the shoulder appearing at higher temperature 678 K, indicates the presence of carbon graphite in less extension.

Quantification of methane was obtained by integration of the signal from the mass spectra (ratio e/m=15). The correlation with methane pulses at different adsorption temperatures permitted to calculate the moles of methane evolved during the hydrogenation. . The quantitative results presented in Table 1 show that, despite the formation of less reactive species, the adsorption capacity of the PdSON catalyst increases tenfold with increasing chemisorption temperature from 423 K to 623 K. The adsorption capacity (μmols of CH_4 per gram of catalyst) of the PdCOL is higher than of the PdSON catalyst.

Figure 11 displays the Arrhenius plot of the CH_4 adsorption capacity and the energy of activation. Results show that the energy of activation of the PdCOL is 18.8 KJ/mol, while of the PdSON catalyst it is 29.4 KJ/mol. Indeed, the adsorption barrier in the PdSON catalyst is approximately 10 KJ/mol higher than of the PdCOL catalyst.

Martins et al. [28] showed similar behavior considering the reactivity of methane for adsorption on Pd surfaces. These authors obtained 0.2 and 8 μmoles/g of catalyst with 5% of Pd. Here we found similar values but with 1% Pd content (w/w). The adsorption capacity is higher and practically five times higher when compared to the previous work. Indeed, comparing the dispersions or particle sizes the PdSON catalyst presents small particles, which may favor the adsorption capacity of methane and reactivity of carbon adspecies at lower temperature. The PdCOL catalyst displayed larger particles, however, from the TPD results the adsorption capacity occurs at a larger range of temperature, which may favor the adsorption capacity at an extended temperature range.

Selectivity- Non oxidative coupling of methane in two steps

The catalytic tests for the non oxidative coupling of methane were performed isothermally, similar to methodology described by Belgued et al. [1, 3, 6, 29] and Amariglio et al. [30-31]. Details of this methodology were also reported by Martins et al. [9] and Moya et al. 17]. Briefly, approximately 100 mg of the catalyst was reduced at 773 K. Pure methane was adsorbed at temperatures between 523 and 823 K for one min. Then, after purging, hydrogenation of carbon residues was performed with pure H_2 at high flow rates for 1 min.

The results are displayed in Figures 12 and 13 for PdSON and PdCOL, respectively. These results are presented in terms of selectivity (carbon basis) considering the total amount of products after two steps. The excess of methane limited the analyses of methane and we assumed 100% (carbon basis) all products originated from the coupling reaction in steps 1 and 2. Quantitatively the adsorbed methane was determined through TPSH.

Both catalysts showed evolution of H_2 during the chemisorption of methane for all temperatures. During methane adsorption on PdSON the products released were ethane and propane, as shown in figure 12A, however, propane decreased with increasing temperature. The initial selectivity was 2.8%.The selectivity of ethane was 12% at 423 K but also decreased with temperature to 9%. The maximum selectivity of C_2^+ was 18% for temperatures of 673 K and 723 K, which are better than those reported in the literature with noble metals. Amariglio et al. [31] obtained 12-13%. Only traces of ethylene were detected above 723K. In the hydrogenation step we observed major methane formation due to the hydrogenation of carbon residues at the surface, as shown in figure 12B.

On the contrary, for the PdCOL catalyst ethane (C_2^+) was not observed during the adsorption step of methane. In the hydrogenation step in majority methane was produced but also ethane (Figure 13). The selectivity of ethane increased from 4% to 8% between 473 K and 523 K but remained constant till 773 K. The formation of ethane in this step evidences reactivity but does not activity for coupling reaction at the surface. Ethane formation may occur in the gas phase reaction, in accordance with the literature [1, 21].

Discussion

The results for non oxidative methane coupling on Pd catalysts tested here showed high catalytic activity for methane coupling. We observed the formation of C_2 and C_3 at 473 K. In majority methane was observed after the hydrogenation of carbon species at the surface.

DRIFTS and TPD results of CO adsorption support the coupling-hydrogenolysis reactions. On the other hand, TEM results showed that the PdSON catalyst presented smaller and narrower distribution of Pd particles at the surface than PdCOL that displayed larger and less dispersed Pd particles, which probably influence the coupling-hydrogenolysis process. The formation of C_2^+ in the first step on PdSON evidences high activity of reactive carbon adspecies. However, aging carbon species that probably may occur during the experiment disfavor C-C coupling in the second step. Studies with platinum supported catalysts showed that the activity increases with decreasing particle size, but the product distribution increased toward higher hydrocarbons (MA et al [10]).

The PdCOL and PdSON catalysts presented different dispersions and selectivities in accordance with WINSLOW *et al.* [26]. They suggested reaction sensibility in the homologation-hydrogenolysis process as function of the dispersion of the active phase. Indeed, the PdSON catalyst formed C_2 and C_3 and therefore allowed the occurrence of surface coupling reaction, while the PdCOL catalyst did not. On the opposite, ethane was produced in the hydrogenation step in the gas phase.

The activity results and surface particles confirmed the hypothesis raised by Koerts et al [25] that the surface with higher dispersed particles and with lots of metallic sites in positions of low coordination, such as corners and edges, generate highly reactive systems favoring the hydrogenolysis.

As reported by Belgued et al. [29], the amount of higher hydrocarbons obtained is strongly dependent upon the pressure and the flow rate of CH_4 during the first step of the

process. The flow rates of methane affect the composition of the chemisorbed layer built up during the gas exposition and high flow rate acts as dehydrogenating agent by conveying the desorbed H_2 out, moving forward the equilibrium of methane chemisorption. H_2 evolution resulted from methane dissociative chemisorption, followed by the associative desorption of H_{ads}. The parallel evolution of ethylene and ethane, in the same way, may be attributed to the associative desorption of two adsorbed methyl or methylene groups [9]:

$$2CH_{3;ads} \rightarrow C_2H_6 + 2*$$

$$2CH_{2;ads} \rightarrow C_2H_4 + 2*$$

Propane evolution means that C–C bond formation occurs during methane chemisorption:

$$CH_3CH_{ads} \rightarrow CH_{3;ads} \rightarrow C_3H_8 + 2*$$

Propylene as well as ethylene evolutions were not observed as the results from the propane and ethane dehydrogenation at the metal surface.

These results confirm that the reactions are strongly dependent of the particle sizes and nano sized particles affect the coupling-hydrogenolysis process.

Conclusions

Two different samples of Pd on α-Al_2O_3 catalysts with Pd particles in the low nanometer range have been prepared by a sonochemical reduction and a colloidal method, respectively. The two catalysts differ in their particle size and the widths of their particle size distributions, the latter exhibiting a broader distribution of in average larger particles and a less homogeneous distribution of Pd particles over the support. Also the adsorptive properties of the Pd/Al_2O_3 samples are different as a result of the different preparation methods. CO, which is preferable linearly adsorbed on the metallic Pd surface, is less strongly bound and thus upon heating less reactive towards desproportionation on the sample with the smaller particles.

Interestingly, the methane adsorption capacity (μmols of CH_4 per gram of catalyst) of that sample is lower than that of the catalyst with larger particles and the energy of activation is nearly doubled.

The catalytic activity evidenced different adspecies formation and methane coupling during chemisorption on both catalysts. During the hydrogenation the carbon adspecies formed majority methane at low adsorption temperatures. These carbon adspecies evidenced different C phases, which are reactive at higher temperatures. The significant amount of adsorbed methane at 773 K is governed by the highly active coordination unsaturated sites at the surface. These results confirm that the reactions are strongly dependent of the particle sizes and nano sized particles affects the coupling-hydrogenolysis process.

References

(1) M. Belgued, P. Paréja, A. Amariglio, Nature 352 (1991) 789-790.

(2) T. Koerts, M.J.A. Deelen, R.A. van Santen, R.A., J. Catal. 138 (1992) 101-114.

(3) M. Belgued, A. Amariglio, P. Paréja, H. Amariglio, J. Catal. 159 (1996) 441-448.

(4) M. Belgued, A. Amariglio, P. Paréja, H. Amariglio, J. Catal. 159 (1996) 441-449.

(5) P. Paréja, S. Molina, A. Amariglio, H. Amariglio, Appl. Catal.A 168 (1998) 289-305.

(6) M. Belgued, A. Amariglio, L. Lefort, P. Paréja, H. Amariglio, J. Catal. 161 (1996) 282-291.

(7) O. Garnier, J. Shu, B.P.A. Grandjean, Ind. Eng. Chem. Res. 36 (1997) 553-558.

(8) L.Guczi, L. Borkó, Catal. Today 64 (2001) 91-96.

(9) R. L. Martins, M. A.S. Baldanza, M. M.V.M. Souza and M. Schmal, Appl. Catal. A: General 318 (2007) 207–212.

(10) J. Ma, S. Reng, D. Pan, R.Li, K. Xie, Reac. Func. Pol., 62 (2005) 31-39.

(11) K.S. Suslick, T. Hyeon, M. Fang, A.A. Cichowlas, Mater. Sci. Eng. A 204 (1995) 186-192.

(12) K.Okitsu, A.Yue, S.Tanabe, H. Matsumoto, Chem. Mater. 12 (2000) 3006-3011.

(13) N.A.Dhas, A. Ekhtiarzadeh, K.S. Suslck, 2001, J. Amer. Chem. Soc. 123(2001) 8310-8316.

(14) H.Li, R.Wang, . Hong, L. Chen, Z.Zhong, Y. Koltypin, J.Calderon-Moreno, A.Gedanken, Langmuir, 20 (2004) 8352-8356.

(15) A.Miyazaki, I. Balint, Y. Nakano, J. Nanop. Res., 5 (2003) 69-80.

(16) K.Okitsu, A. Yue, S. Tanabe, H. Matsumoto, Chem.Mater., 12 (2000b) 3006-3011.

(17) S.F.Moya, R.L.Martins, M. Schmal, Appl. Catal.A: Gen., 396 (2011) 159–169.

(18) Unterhalt, Analytica Chimica Acta, 452 (2002) 1-31.

(19)R.P.Eischens, Infrared spectra of chemisorbed molecules, doi/10.1002/bbpc.19560600805/abstract, 1956.

(20) A. Palazov, C. Chang, P. Kokes, J, Catal., 36, 338 (1975) 4.

(21) S.Ichikawa, H. Poppa, M. Boudart, J. Catal., 91(1985) 1-10.

(22) H.Dropsch, M. Baerns, Appl. Catal. A¸ 158 (1997) 163-183.

(23) R.S.Monteiro, L.C. Dieguez, M. Schmal, Catal.Today, 65 (2001) 77-89.

(24) G.Panzera, V. Modafferi, S. Candamano, A.Donato, F.Frusteri, P.L.Antonucci, J. of Power Sources, 135 (2004)177-183.

(25) T. Koerts, N.R.A.Van Santen, J. Mol. Catal., 74 (1992) 185-191.

(26) P.Winslow, A.T. Bell, J. Catal. 86 (1984) 158-172.

(27) Y.Lu, Z. Xiong, J.Li, J. Lin, Catal. Lett. 76 (2001) 167-175.

(28) R.L. Martins, M.A. Baldanza, M.V.M. Souza, M.Schmal, Stud. Surf. Sci. Catal. 147 (2004) 643-648.

(29) M.Belgued, H. Amariglio, P. Pareja, A. Amariglio J.Saintjust, Catal.Today 13 (1992) 437-445.

(30) A.Amariglio, P Pareja, M. Belgued, H. Amariglio, J. Chem. Soc., Chem. Commun., (1994) 561-562.

(31) A.Amariglio, M. Belgued, P. Pareja, H. Amariglio, J. Catal. 177 (1998) 113-120.

Caption of figures

Figure 1: Diffractogram of PdSON. Red lines are diffractions of metallic Pd. (*****) lines correspond to α-Al_2O_3, and (**!**) lines to aluminum silicate.

Figure 2 – Diffractogram of α-alumina (A), PdCOL before calcination (B) and (C) after calcination. Blue lines are diffractions of bulk metallic palladium.

Figure 3: TEM images of PdSON after preparation.

Figure 4: TEM images of PdSON after reduction with H_2 at 673 K.

Figure 5 – Images of the PdCOL sample before and after calcinations.

Figure 6 – Histogram of the PdSON reduced sample (A) and of PdCOL sample after reduction (B).

Figure 7 – DRIFTS results of CO on PdCOL (A) PdSON (B) after CO adsorption and after He flux at 298K.

Figure 8 - TPD CO on PdSON (A) and PdCOL (B).

Figure 9: TPSR of H_2 on PdSON after chemisorption of methane at: 473K

(**A**);563K (**B**) and; 673K (**C**).

Figure 10: TPSR of H_2 on PdCOL after chemisorption of methane at: 473K

(**A**);563K (**B**) and; 673K (**C**).

Figure 11 – Arrhenius plot of PdSON and PdCOL .

Figure 12 A – Selectivity after the chemisorption of methane for the PdSON catalyst (step1).

Figure 12 B – Selectivity after hydrogenation for the PdSON catalyst (step 2).

Figure 13 - Selectivity for the PdCOL catalyst after chemisorption and hydrogenation step.

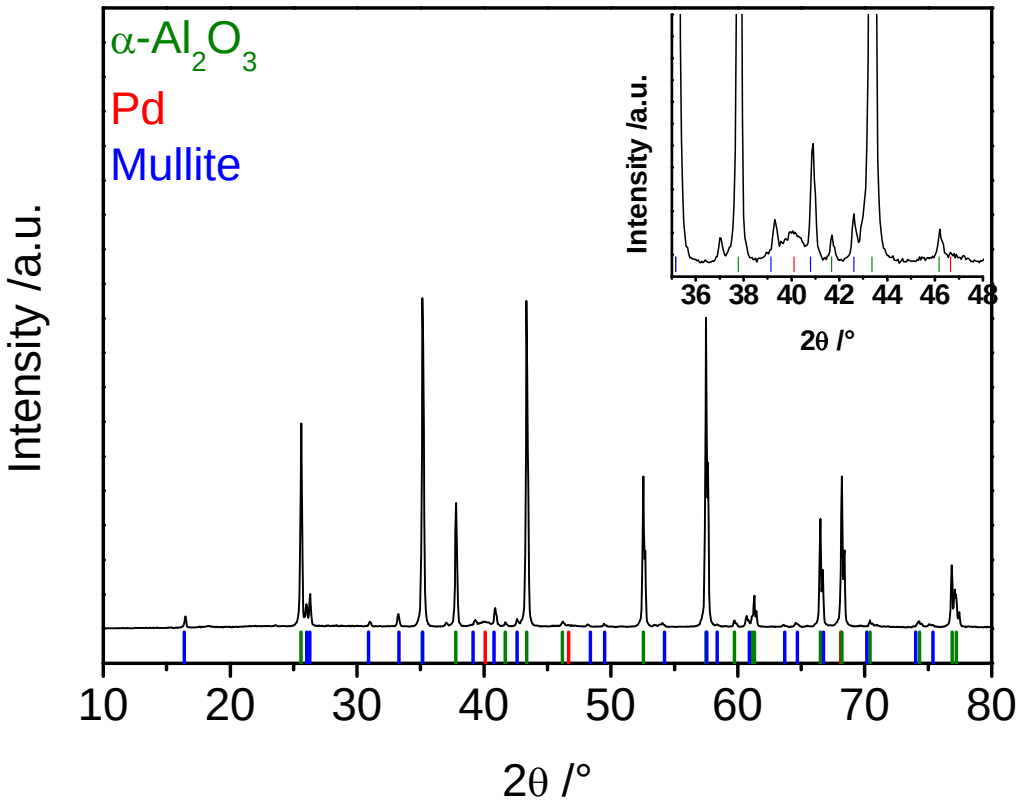
α-Al2O3
Pd
Mullite
Intensity /a.u.
2θ /°
10
20
30
40
50
60
70
80
Intensity /a.u.
2θ /°
36
38
40
42
44
46
48

Figure 1

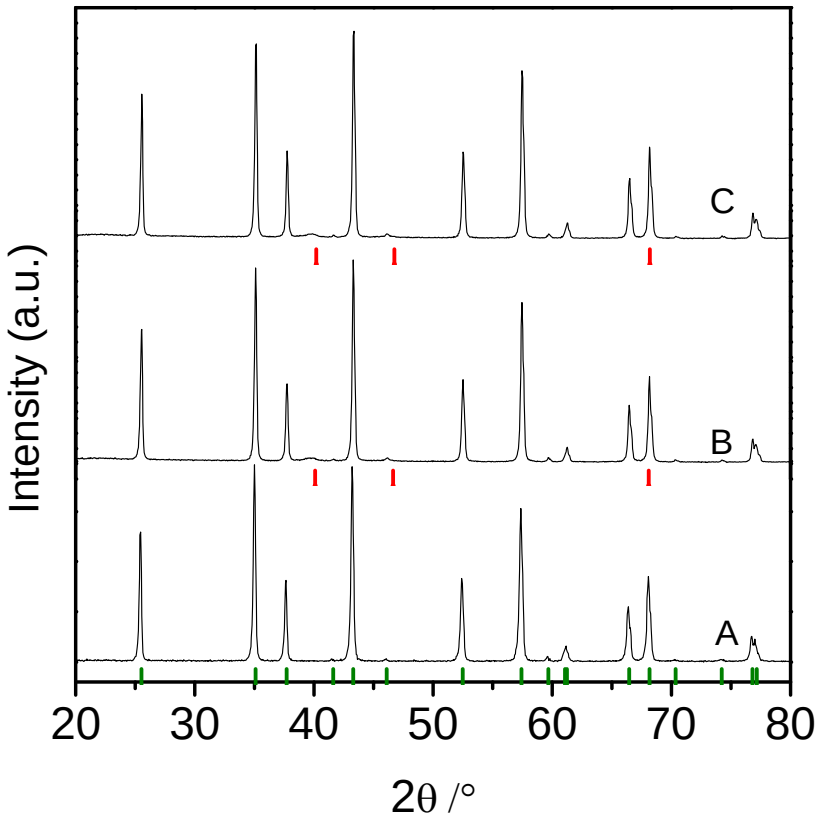

Figure 2

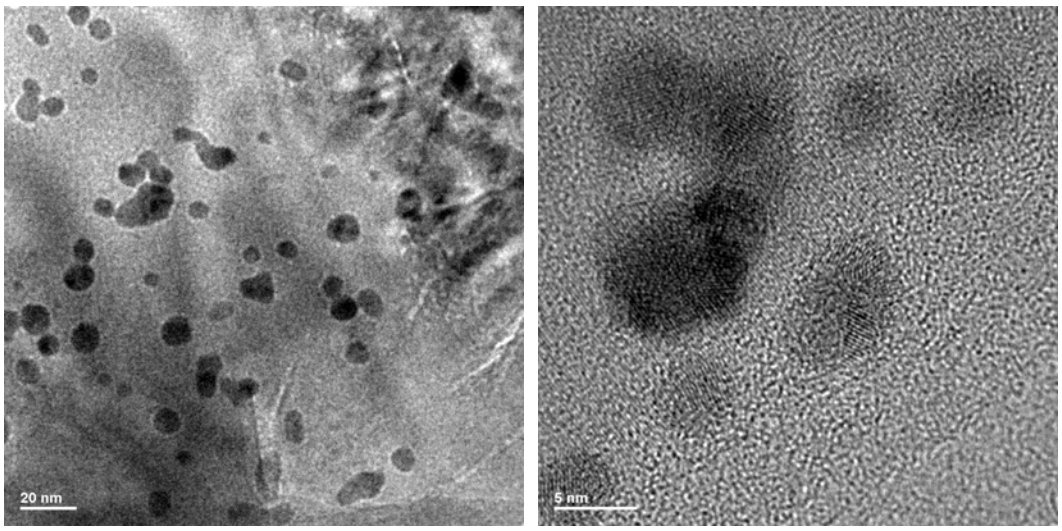

Figure 3

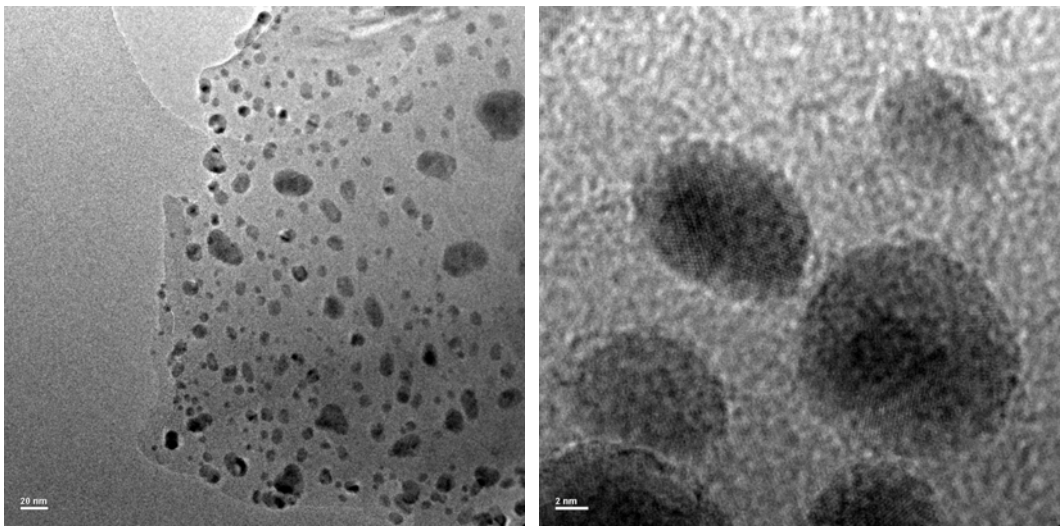

Figure 4

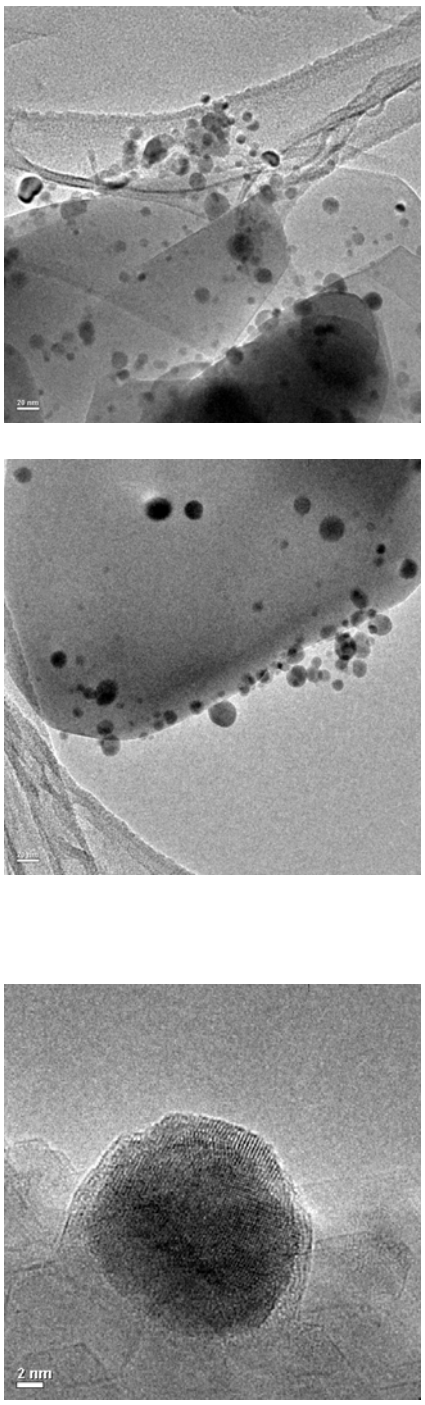

Figure 5

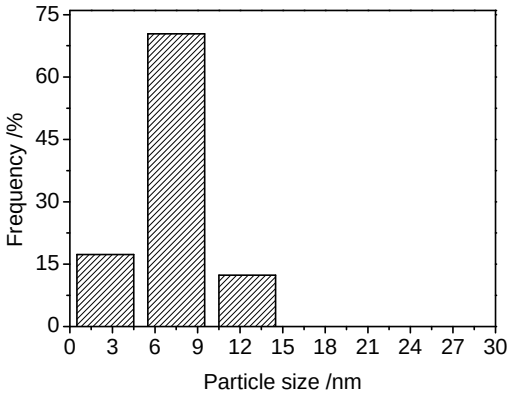

Figure 6A

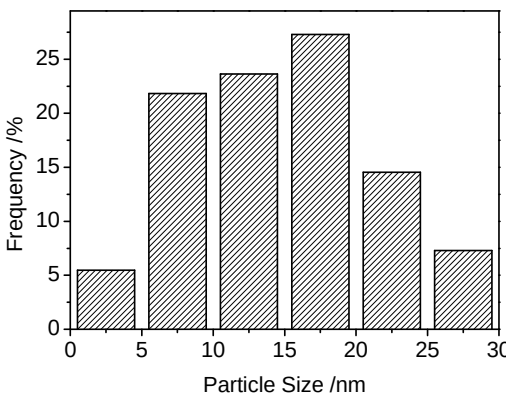

Figure 6B

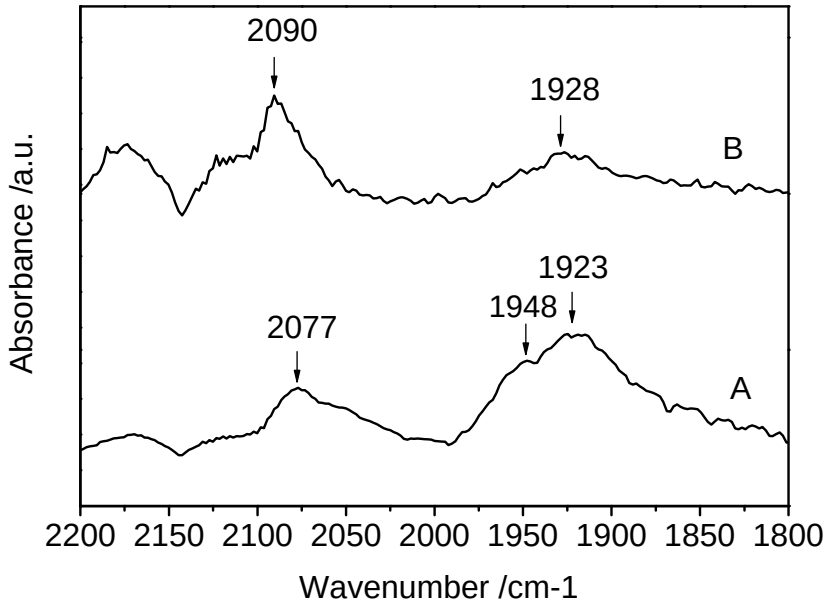
2090
1928
B
1923
1948
2077
A
Absorbance /a.u.
2200 2150 2100 2050 2000 1950 1900 1850 1800
Wavenumber /cm-1

Figure 7

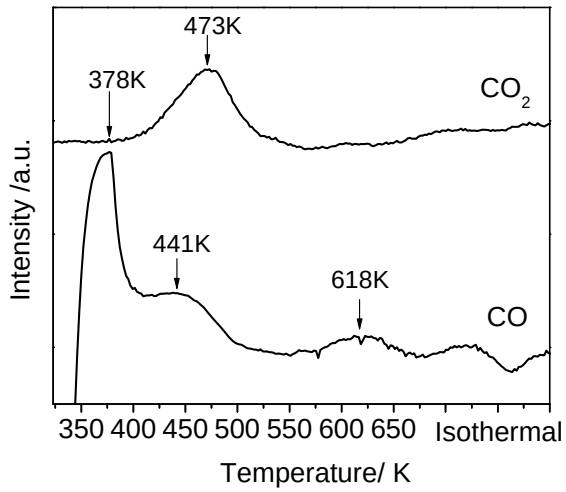

Figure 8A

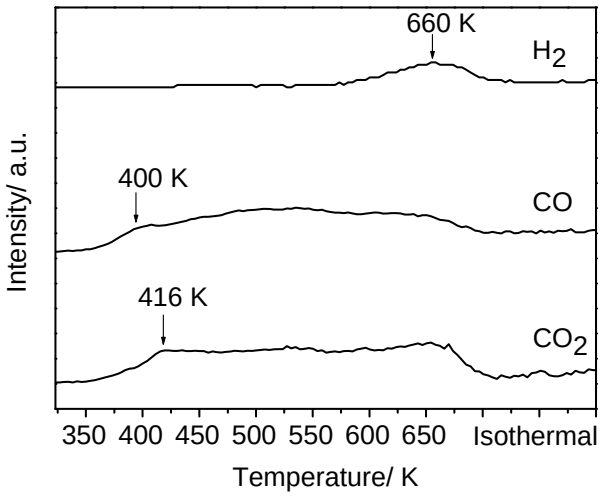

Figure 8B

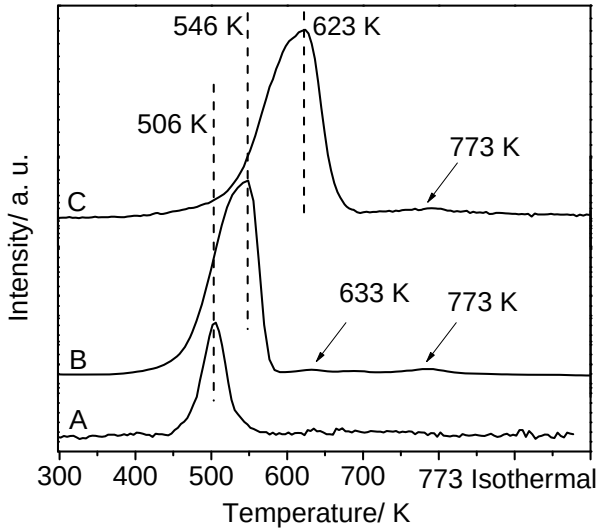

Figure 9

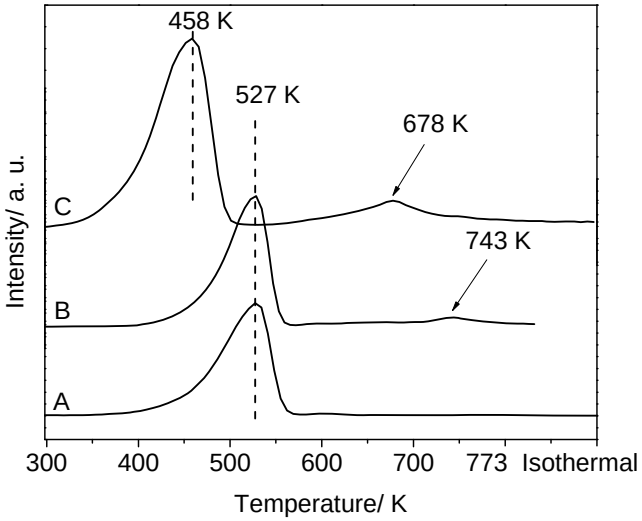

Figure 10

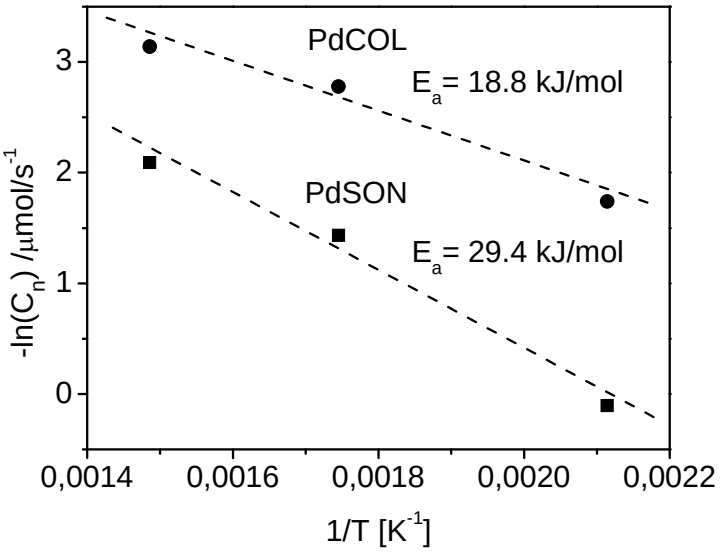
PdCOL
E_a = 18.8 kJ/mol
PdSON
E_a = 29.4 kJ/mol
-ln(C_n) /μmol/s^-1
1/T [K^-1]
3
2
1
0
0,0014
0,0016
0,0018
0,0020
0,0022

Figure 11

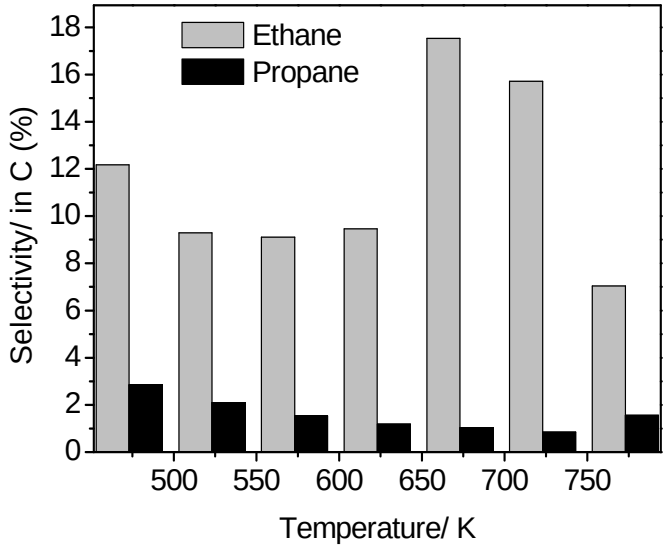

igure 12A

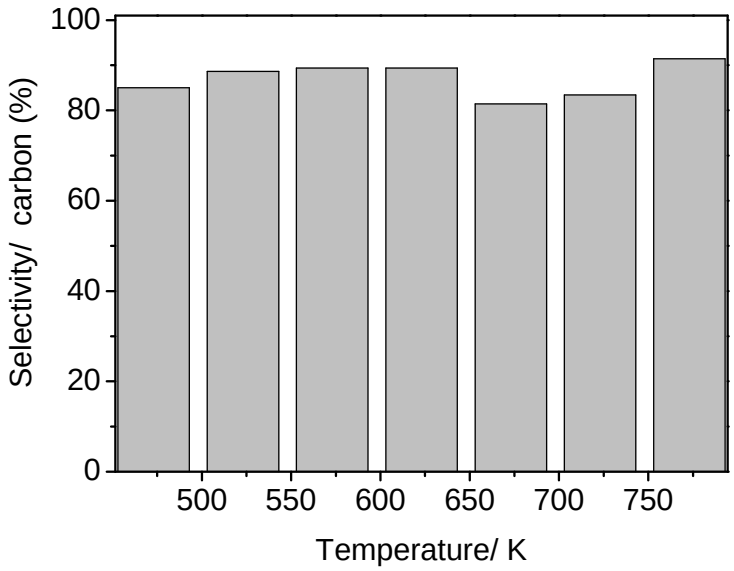

Figure 12B

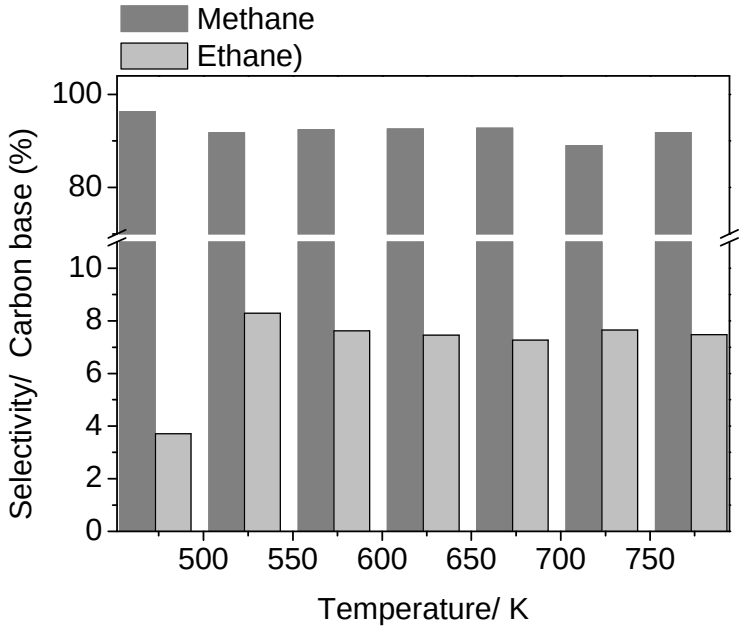
Methane
Ethane)
100
80
10
8
6
4
2
0
Selectivity/ Carbon base (%)
500
550
600
650
700
750
Temperature/ K

Figure 13

Table 1:

Catalysts	**$T_{Adsorption\ Methane}$**	**Total $C_{hydrogenated}$ [$\mu mol/g_{cat}$]**
PdSON	473K	0.9
	573K	4.2
	673K	8.1
PdCOL	473K	5.7
	573K	16.1
	673K	23.1